43. Tanzawa Y, Tsuchiya H, Yamamoto N, Sakayama K, Minato H, Tomita K. Histological examination of frozen autograft treated by liquid nitrogen removed 6 years after implantation. *J Orthop Sci.* 2008;13:259–264.
44. Terunuma H, Deng X, Dewan Z, Fujimoto S, Yamamoto N. Potential role of NK cells in the induction of immune responses: implications for NK cell-based immunotherapy for cancers and viral infections. *Int Rev Immunol.* 2008;27:93–110.
45. Toes RE, Blom RJ, Offringa R, Kast WM, Melief CJ. Enhanced tumor outgrowth after peptide vaccination: functional deletion of tumor-specific CTL induced by peptide vaccination can lead to the inability to reject tumors. *J Immunol.* 1996;156:3911–3918.
46. Tsuchiya H, Tomita K, Mori Y, Asada N, Morinaga T, Kitano S, Yamamoto N. Caffeine-assisted chemotherapy and minimized tumor excision for nonmetastatic osteosarcoma. *Anticancer Res.* 1998;18:657–666.
47. Tsuchiya H, Tomita K, Mori Y, Asada N, Yamamoto N. Marginal excision for osteosarcoma with caffeine assisted chemotherapy. *Clin Orthop Relat Res.* 1999;358:27–35.
48. Tsuchiya H, Wan SL, Sakayama K, Yamamoto N, Nishida H, Tomita K. Reconstruction using an autograft containing tumour treated by liquid nitrogen. *J Bone Joint Surg Br.* 2005;87:218–225.
49. Tsuchiya H, Yasutake H, Yokogawa A, Baba H, Ueda Y, Tomita K. Effect of chemotherapy combined with caffeine for osteosarcoma. *J Cancer Res Clin Oncol.* 1992;118:567–569.
50. Urano M, Tanaka C, Sugiyama Y, Miya K, Saji S. Antitumor effects of residual tumor after cryoablation: the combined effect of residual tumor and a protein-bound polysaccharide on multiple liver metastases in a murine model. *Cryobiology.* 2003;46:238–245.
51. Visonneau S, Cesano A, Jeglum KA, Santoli D. Adjuvant treatment of canine osteosarcoma with the human cytotoxic T-cell line TALL-104. *Clin Cancer Res.* 1999;5:1868–1875.
52. Warren RQ, Tsang KY. Induction of immunity to a human osteosarcoma-associated antigen in mice using anti-idiotypic antibodies. *Clin Immunol Immunopathol.* 1990;56:334–343.
53. Yamamoto N, Tsuchiya H, Tomita K. Effects of liquid nitrogen treatment on the proliferation of osteosarcoma and the biomechanical properties of normal bone. *J Orthop Sci.* 2003;8:374–380.

Published OnlineFirst July 27, 2010; DOI:10.1158/0008-5472.CAN-10-0096

AACR

Cancer Research

Antitumor Effect after Radiofrequency Ablation of Murine Hepatoma Is Augmented by an Active Variant of CC Chemokine Ligand 3/Macrophage Inflammatory Protein-1α

Noriho Iida, Yasunari Nakamoto, Tomohisa Baba, et al.

Cancer Res 2010;70:6556-6565. Published OnlineFirst July 27, 2010.

Published OnlineFirst July 27, 2010; DOI:10.1158/0008-5472.CAN-10-0096

Therapeutics, Targets, and Chemical Biology

Cancer Research

Antitumor Effect after Radiofrequency Ablation of Murine Hepatoma Is Augmented by an Active Variant of CC Chemokine Ligand 3/Macrophage Inflammatory Protein-1α

Noriho Iida[1], Yasunari Nakamoto[1], Tomohisa Baba[2], Hidetoshi Nakagawa[1], Eishiro Mizukoshi[1], Makoto Naito[3], Naofumi Mukaida[2], and Shuichi Kaneko[1]

Abstract

Several chemokines are used for immunotherapy against cancers because they can attract immune cells such as dendritic and cytotoxic T cells to augment immune responses. Radiofrequency ablation (RFA) is used to locally eliminate cancers such as hepatocellular carcinoma (HCC), renal cell carcinoma, and lung cancer. Because HCC often recurs even after an eradicative treatment with RFA, additional immunotherapy is necessary. We treated tumor-bearing mice by administering ECI301, an active variant of CC chemokine ligand 3, after RFA. Mice were injected s.c. with BNL 1ME A.7R.1, a murine hepatoma cell line, in the bilateral flank. After the tumor became palpable, RFA was done on the tumor of one flank with or without ECI301. RFA alone eliminated the treated ipsilateral tumors and retarded the growth of contralateral non–RFA-treated tumors accompanied by massive T-cell infiltration. Injection of ECI301 augmented RFA-induced antitumor effect against non–RFA-treated tumors when administered to wild-type or *CCR5*-deficient but not *CCR1*-deficient mice. ECI301 also increased CCR1-expressing $CD11c^+$ cells in peripheral blood and RFA-treated tumors after RFA. Deficiency of *CCR1* impairs accumulation of $CD11c^+$, $CD4^+$, and $CD8^+$ cells in RFA-treated tumors. Furthermore, in IFN-γ-enzyme-linked immunospot assay, ECI301 augmented tumor-specific responses after RFA whereas deficiency of *CCR1* abolished this augmentation. Thus, we proved that ECI301 further augments RFA-induced antitumor immune responses in a CCR1-dependent manner. *Cancer Res; 70(16); 6556–65. ©2010 AACR.*

Introduction

Chemokines are a class of candidate molecules for immunotherapy. Chemokines are presumed to play an essential role in the regulation of leukocyte trafficking and dendritic cell-T-cell interactions (1–4). In animal experiments, intratumoral use of chemokines, such as monocyte chemoattractant protein-1/CC chemokine ligand 2 (CCL2), macrophage inflammatory protein (MIP)-1α/CCL3, or MIP-3α/CCL20, succeeds in decreasing tumorigenesis accompanied by increase in the numbers of tumor-infiltrating dendritic, natural killer, or T cells (5–7). Thus, application of chemokines in immunotherapy is promising but needs further refinement before they can be used in clinical situations.

Radiofrequency ablation (RFA) is an eradicative treatment against cancers, such as hepatocellular carcinoma (HCC), renal cell carcinoma, and lung cancer. RFA of HCC can generate HCC-specific T cells in peripheral blood (8). Activation of dendritic cells in human peripheral blood is also observed after this treatment (9). Thus, RFA can induce immunogenic tumor cell death and subsequently tumor-specific immune responses (8–11). However, multicentric development of HCC in the cirrhotic liver frequently results in tumor recurrence even after the apparent curative treatment of HCC by RFA (12). These observations suggest that RFA-induced tumor-specific immune responses are often not sufficient to prevent tumor recurrence. Thus, additional treatment modalities are required to augment HCC-specific immune responses.

CCL3/MIP-1α can augment immune responses but problems arise because of its tendency to form large aggregates at high concentrations when administered systemically. Unlike human naïve CCL3, BB-10010 is generated by a single amino acid substitution of Asp26 to Ala and exhibits similar biological potencies, but rarely forms large aggregates (13). Based on its activity to mobilize bone marrow cells to peripheral blood, randomized clinical trials were performed to examine whether the combined administration of BB-10010 and chemotherapeutic agents can protect against chemotherapy-induced neutropenia. However, the myeloprotective effects of BB-10010 were not sufficient to warrant its use with chemotherapy (14). Concomitantly, several lines of evidence reveal that the administration of human recombinant CCL3

Authors' Affiliations: [1]Disease Control and Homeostasis, Graduate School of Medical Science, and [2]Division of Molecular Bioregulation, Cancer Research Institute, Kanazawa University, Kanazawa, Japan; and [3]Division of Cellular and Molecular Pathology, Niigata University Graduate School of Medicine, Niigata, Japan

Corresponding Author: Shuichi Kaneko, Disease Control and Homeostasis, Graduate School of Medical Science, Kanazawa University, 13-1 Takara-machi, Kanazawa 920-8641, Japan. Phone: 81-76-265-2235; Fax: 81-76-234-4250; E-mail: skaneko@m-kanazawa.jp.

doi: 10.1158/0008-5472.CAN-10-0096

Published OnlineFirst July 27, 2010; DOI:10.1158/0008-5472.CAN-10-0096

can mobilize activated T-cell and dendritic cell precursors into circulation (15, 16).

ECI301, which has the same amino acid sequence as BB-10010, was generated using the fission yeast (*Schizosaccharomyces pombe*) expression system. ECI301 can augment irradiation-induced tumor regression when administered systemically to mice bearing multiple subcutaneous tumors (17). Of interest is the fact that the effects were observed in both unirradiated and irradiated tumors. Thus, systemic ECI301 treatment can augment irradiation-induced tumor-specific systemic immunity. These observations prompted us to investigate the effects of ECI301 on RFA-treated mice. Here, we show that ECI301 further augments RFA-induced antitumor immune responses in a CCR1-dependent manner.

Materials and Methods

Mice

Seven- to 9-week-old specific pathogen–free female BALB/c mice were purchased from Charles River Japan and designated as wild-type (WT) mice. BALB/c-*nu/nu* mice were purchased from CLEA Japan. *CCR1*-deficient (*CCR1*$^{-/-}$) mice were a gift from Dr. Philip M. Murphy (National Institute of Allergy and Infectious Disease, NIH, Bethesda, MD); *CCR5*-deficient (*CCR5*$^{-/-}$) mice were a gift from Dr. Kouji Matsushima (Department of Molecular Preventive Medicine, Tokyo University, Tokyo, Japan). All mice were backcrossed to BALB/c mice for 8 to 10 generations. All animal experiments were performed under specific pathogen–free conditions in accordance with the Guidelines for the Care and Use of Laboratory Animals of Kanazawa University (Japan).

Tumor cell line

A murine HCC cell line, BNL 1ME A.7R.1 (BNL), was purchased from the American Type Culture Collection in 1998 and kept at low passage throughout the study. The cells were screened for bacteria, fungus, and *Mycoplasma* contamination by direct culture method in 2006 before start of the study. The cells were cultured in DMEM (Sigma Chemical Co.) containing 10% fetal bovine serum (FBS), 0.1 mmol/L nonessential amino acids, 1 μmol/L sodium pyruvate, 2 mmol/L L-glutamine, 50 μg/mL streptomycin, and 100 units/mL penicillin (Life Technologies, Inc.).

Animal models

ECI301 was generated as previously described and provided by Effector Cell Institute, Inc. (17, 18). The left and right flanks of 7- to 9-week-old female WT, *CCR1*$^{-/-}$, *CCR5*$^{-/-}$, and *nu/nu* mice were injected s.c. with 5×10^5 BNL cells in 100 μL of PBS. Fourteen days later, when tumor size reached a diameter of 6 to 8 mm, tumors of one flank were treated using a radiofrequency generator (RITA 500PA, RITA Medical Systems) and needle as described below. On days 0, 2, and 4 after RFA, 20 μg of ECI301 in 100 μL of PBS were injected i.v. via the tail vein, whereas mice treated with RFA alone were injected with 100 μL of PBS. Untreated tumor-bearing mice were used as controls. In another schedule, 2 μg of ECI301 in 100 μL of PBS were injected i.v. from day 0 to day 4 (5 consecutive days). The sizes of non–RFA-treated tumors on the contralateral flank were evaluated twice a week using calipers, and tumor volumes were calculated using the following formula: tumor volume (mm^3) = (longest diameter) × (shortest diameter)^2 / 2.

RFA-treated or non–RFA-treated tumors were excised at the indicated time intervals for immunohistochemical analysis and quantitative real-time reverse transcription-PCR (RT-PCR). Spleens and peripheral blood were removed from the mice at the indicated time intervals for flow cytometric analysis and enzyme-linked immunospot assay (ELISPOT).

Radiofrequency ablation

Mice were anesthetized by i.p. injection of Somnopentyl (Schering-Plough Animal Health) and carefully shaved in the tumor area. After placing the mice onto an aluminum plate attached with an electricity-conducting pad, an RFA needle of expandable electrode with maximum dimension of 20 mm (70SB 2 cm; RITA Medical Systems) was inserted into the middle of the tumors and expanded at 2 or 3 mm. RFA treatments were done using a radiofrequency generator at a power output of 25 W for 1.5 minutes and the temperature of the needle tips reached 70°C to 80°C.

Immunohistochemical analysis

The removed tumor tissues were embedded in Sakura Tissue-Tek optimum cutting temperature (OCT) compound (Sakura Finetek) as frozen tissues. Cryostat sections of the frozen tissues were fixed with 4% paraformaldehyde in PBS and stained with rat anti-mouse CD4 (BD Biosciences), rat anti-mouse CD8a (BD Biosciences), hamster anti-mouse CD11c (BD Biosciences), and rat anti-mouse F4/80 antibodies (Serotec) overnight at 4°C. The sections were then incubated with biotinylated rabbit anti-rat IgG (DakoCytomation) or biotinylated mouse anti-hamster IgG (BD Biosciences) for 1 hour at room temperature. The immune complexes were visualized using the Catalyzed Signal Amplification System (DakoCytomation) or the Vectastain Elite ABC and DAB substrate kits (Vector Laboratories) according to the manufacturer's instructions. As a negative control, rat IgG (Cosmo Bio) or hamster IgG (BD Biosciences) was used instead of specific primary antibodies. The numbers of positive cells in each animal were counted in 10 randomly selected fields at 400-fold magnification by an examiner without any prior knowledge of the experimental procedures.

Double-color immunofluorescence analysis

Tumor tissues were embedded in OCT compound as frozen tissues. After fixation with 4% paraformaldehyde/PBS, cryostat sections were stained with the combinations of anti-CD4 and goat anti-mouse CCR1 (Santa Cruz Biotechnology), anti-CD8a and anti-CCR1, anti-F4/80 and anti-CCR1, phycoerythrin (PE)-conjugated hamster anti-CD11c (BD Biosciences) and anti-CCR1, anti-F4/80 and goat anti-mouse CCL3 (R&D Systems), and anti-F4/80 and goat anti-mouse CCL4 antibodies (R&D). After extensive washing, AF488 donkey anti-rat IgG (Invitrogen) was used as a secondary antibody to detect CD4$^+$, CD8a$^+$, or F4/80$^+$ cells. Simultaneously,

Published OnlineFirst July 27, 2010; DOI:10.1158/0008-5472.CAN-10-0096

AF546- or AF488-donkey anti-goat IgG (Invitrogen) was used to detect $CCR1^+$, $CCL3^+$, or $CCL4^+$ cells. The sections were observed using a confocal microscope (LSM 510 META, Zeiss).

Quantitative real-time RT-PCR

Total RNA was extracted from the resected tumor using RNeasy Mini Kit (Qiagen) according to the manufacturer's instructions. After treating the RNA preparations with RNase-free DNase I (Qiagen) to remove residual DNA, cDNA was synthesized as described previously (19). Quantitative real-time PCR was done on a StepOne Real-Time PCR System (Applied Biosystems) using the comparative C_T quantification method. TaqMan Gene Expression Assays (Applied Biosystems) containing specific primers and probes [accession numbers: CCL3, Mm00441258_ml; CCL4, Mm00443111_m1; CCL5, Mm01302428_ml; glyceraldehyde-3-phosphate dehydrogenase (GAPDH), Mm99999915_g1] and TaqMan Fast Universal PCR Master Mix were used with 10 ng of cDNA to quantify the expression levels of CCL3, CCL4, and CCL5. Reactions were performed for 20 seconds at 95°C followed by 40 cycles of 1 second at 95°C and 20 seconds at 60°C. GAPDH was amplified as an internal control and its C_T values were subtracted from the C_T values of the target genes (ΔC_T). The ΔC_T values of tumors after RFA with or without ECI301 were compared with the ΔC_T values of tumors of untreated mice.

Enzyme-linked immunospot assay

To prepare tumor lysates, BNL or CT26 cells were suspended in PBS and subjected to four cycles of rapid freezing in liquid nitrogen and thawing at 55°C. The lysate was spun at 15,000 rpm to remove particulate cellular debris. After harvesting murine spleens on day 21 after RFA, mononuclear cells were isolated by centrifugation through a Histopaque-1083 density gradient (Sigma Chemical). ELISPOT was performed using an IFN-γ-ELISPOT kit (Mabtech). Ninety-six-well plates coated with anti-mouse IFN-γ antibody were blocked for 2 hours with RPMI 1640 (Sigma Chemical) containing 10% FBS. Two hundred fifty thousand splenic mononuclear cells were added in triplicate cultures of RPMI 1640 containing 10% FBS together with BNL or CT26 lysates at a tumor cell-to-mononuclear cell ratio of 2:1. After 48 hours of culture, the plates were washed eight times with sterile PBS and further incubated for 2 hours with biotinylated anti-mouse IFN-γ antibody. After another eight washes, alkaline phosphatase–conjugated streptavidin was added to these

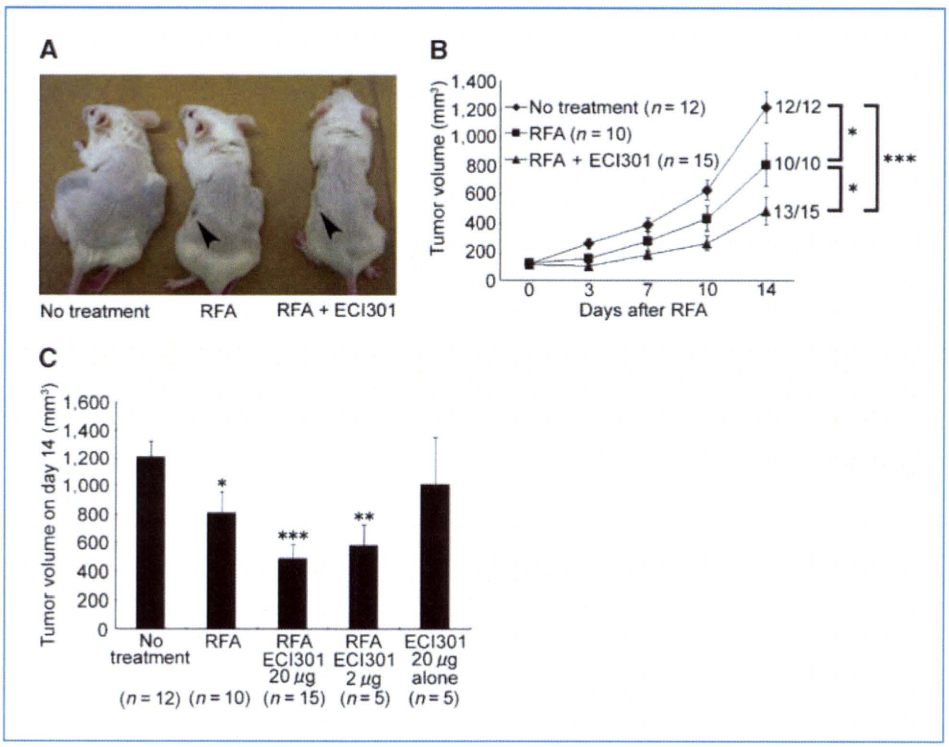

Figure 1. ECI301-induced augmentation of antitumor effects after RFA. WT mice were injected s.c. with 5×10^5 BNL cells into the left and right flanks. Fourteen days later, when tumors became palpable, tumors of one flank were treated using the RFA generator and needle. On day 0, 2, and 4 after RFA, 20 μg of ECI301 in 100 μL of PBS were injected i.v. into each mouse, whereas mice treated with RFA alone were injected with 100 μL of PBS. Tumor-bearing untreated mice were observed as controls. A, macroscopic appearances of the mice on day 14 after RFA are shown. Arrowheads indicate the scar after RFA. Representative results are from at least 10 mice in each group. B, non–RFA-treated tumor volumes after RFA with or without ECI301 were measured twice a week. Points, mean; bars, SE. *, $P < 0.05$; ***, $P < 0.001$. C, volumes of non–RFA-treated tumors on day 14 after RFA. In addition to the groups described in B, tumor volumes were determined in animals receiving 2 μg of ECI301 in 100 μL of PBS i.v. from day 0 to day 4 (5 consecutive days) after RFA and those receiving 20 μg of ECI301 alone without RFA. Columns, mean; bars, SE. *, $P < 0.05$; **, $P < 0.01$; ***, $P < 0.001$, compared with untreated mice.

Published OnlineFirst July 27, 2010; DOI:10.1158/0008-5472.CAN-10-0096

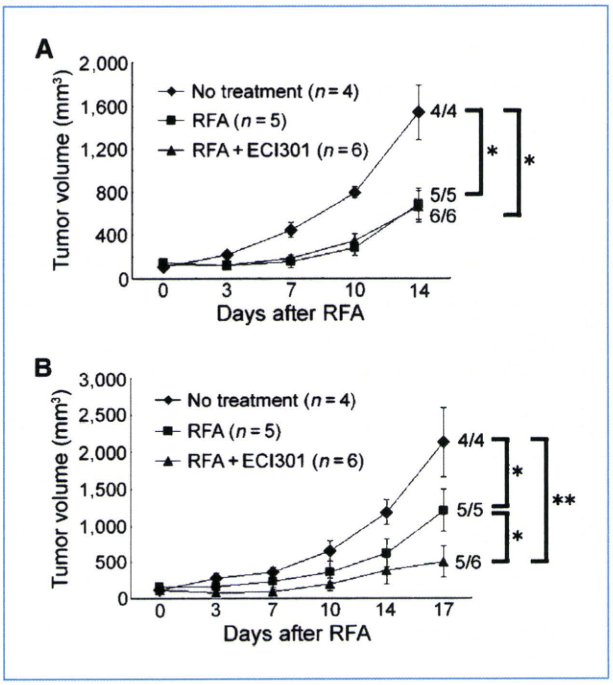

Figure 2. Deficiency of *CCR1* abrogates ECI301-augmented antitumor effects after RFA. $CCR1^{-/-}$ or $CCR5^{-/-}$ mice were inoculated with BNL cells and treated as described in the legend to Fig. 1. Non–RFA-treated tumor volumes were measured twice a week in $CCR1^{-/-}$ (A) and $CCR5^{-/-}$ (B) mice. Points, mean; bars, SE. *, $P < 0.05$; **, $P < 0.01$.

plates and incubated for 1 hour. Finally, the spots were developed with nitroblue tetrazolium/5-bromo-4-chloro-3-indolyl phosphate solution. The number of specific spots was determined by subtracting the number of spots in wells without lysates from the number of spots in wells with tumor lysates. Wells were considered positive if they had more than 10 spots per well and were at least 2-fold greater than control.

Flow cytometric analysis

After harvesting blood samples from mice, mononuclear cells were isolated by centrifugation through a Histopaque-1083 density gradient (Sigma Chemical). The resultant single-cell preparations were stained with various combinations of allophycocyanin (APC)-labeled anti-CD8, APC-labeled anti-CD11c, FITC-labeled anti-CD4 (BD Biosciences), PE-labeled anti-CCR1 (Santa Cruz Biotechnology), and FITC-labeled anti-F4/80 monoclonal antibodies (Serotec). APC-rat IgG, APC-hamster IgG, and FITC-rat IgG were used as isotype controls (BD Biosciences). For each determination, at least 20,000 stained cells were analyzed on a FACSCalibur system (BD Biosciences). The data were expressed as the proportion of positive cells (compared with cells stained with an irrelevant control antibody).

Depletion of macrophages/monocytes

Clodronate liposome was prepared and systemic depletion of monocytes/macrophages was performed as previously described (20, 21). WT mice were i.p. injected with 200 μL of clodronate liposome five times: days −2, 0, 3, 6, and 10 after RFA treatment. Depletion of CD11c-negative monocytes in blood was confirmed by flow cytometry after injection of clodronate liposome.

Statistical analysis

Mean and SD or SE were calculated for the obtained data. Data were analyzed statistically using one-way ANOVA followed by Fisher's protected least significant difference test, except for the data of tumor growth, which were analyzed with two-way ANOVA. $P < 0.05$ was considered statistically significant.

Results

ECI301 augments RFA-induced antitumor effects

To investigate the effects of RFA against RFA-treated and non–RFA-treated tumors, each bilateral flank of BALB/c mice was injected with 5×10^5 BNL cells. Fourteen days later, when tumor size reached a diameter of 6 to 8 mm, tumors of one flank were treated with RFA. On the day after RFA, ulceration occurred in RFA-treated tumors, and these tumors started to shrink (data not shown). On day 14 after RFA, RFA-treated tumors were covered with scars without any macroscopic tumors (Fig. 1A). Moreover, RFA treatment also retarded the growth of contralateral non–RFA-treated tumors compared with the tumors in untreated mice (Fig. 1B and C). ECI301 (20 μg/mouse) administered on days 0, 2, and 4 after RFA augmented RFA-induced growth retardation of contralateral non–RFA-treated tumors (Fig. 1B and C). Furthermore, non–RFA-treated tumors completely disappeared in 2 of 15 mice treated with RFA and ECI301 but not in the other treatment groups (Fig. 1B and C). Therapeutic effects were observed, even when ECI301 (2 μg/mouse) was injected consecutively for 5 days from day 0 to day 4 after RFA.

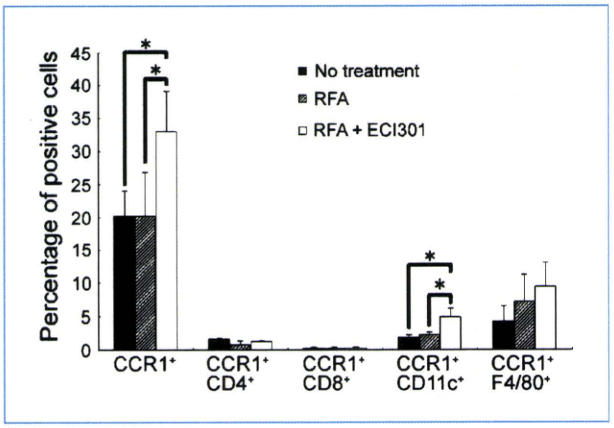

Figure 3. ECI301 increases CCR1-expressing cells in peripheral blood. Peripheral blood sample was harvested 8 h after RFA. Mononuclear cells were separated and stained with the indicated antibodies as described in Materials and Methods. Columns, mean percentages of $CCR1^+$, $CCR1^+CD4^+$, $CCR1^+CD8^+$, $CCR1^+CD11c^+$, or $CCR1^+F4/80^+$ cells ($n = 3$); bars, SD. *, $P < 0.05$.

Published OnlineFirst July 27, 2010; DOI:10.1158/0008-5472.CAN-10-0096

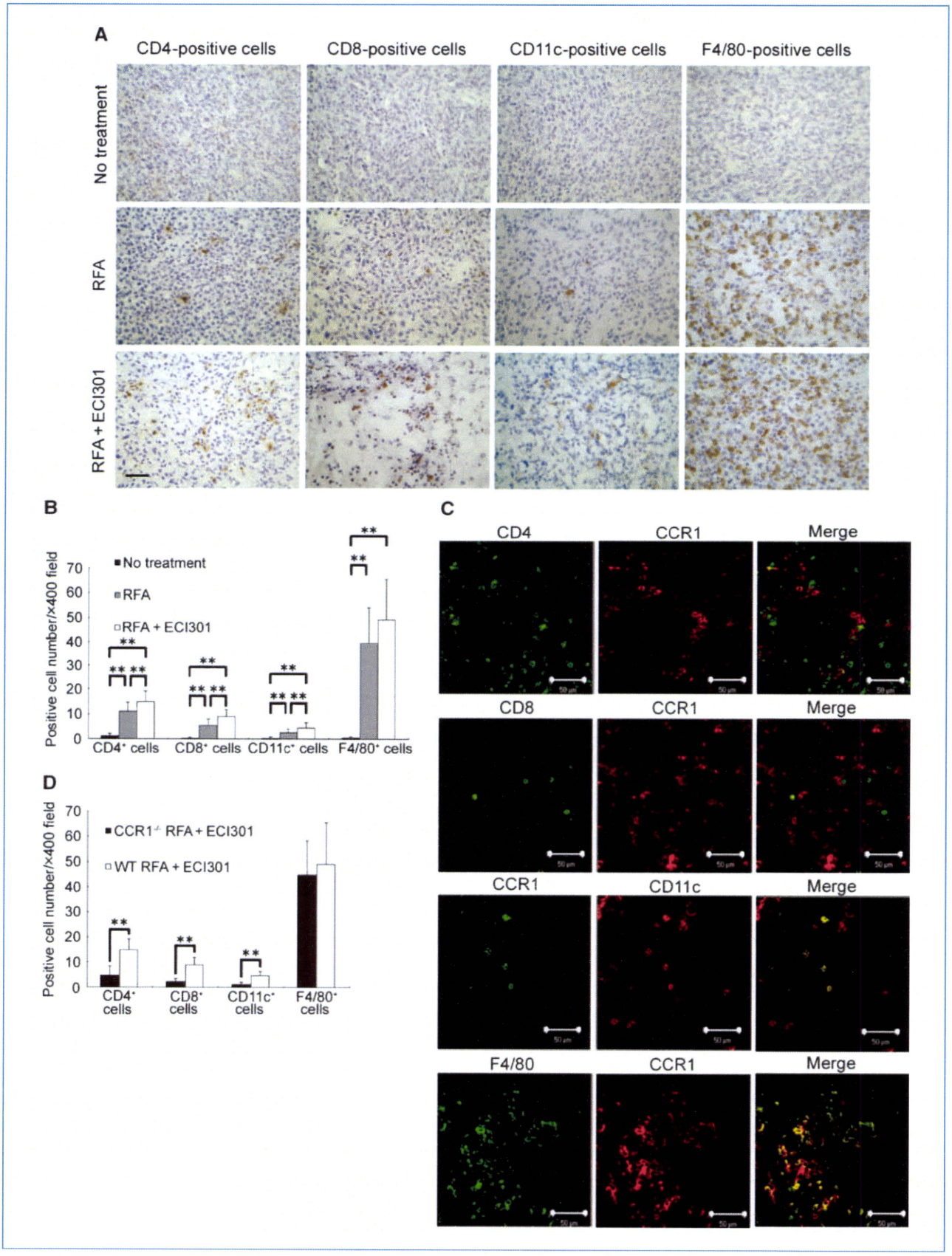

Published OnlineFirst July 27, 2010; DOI:10.1158/0008-5472.CAN-10-0096

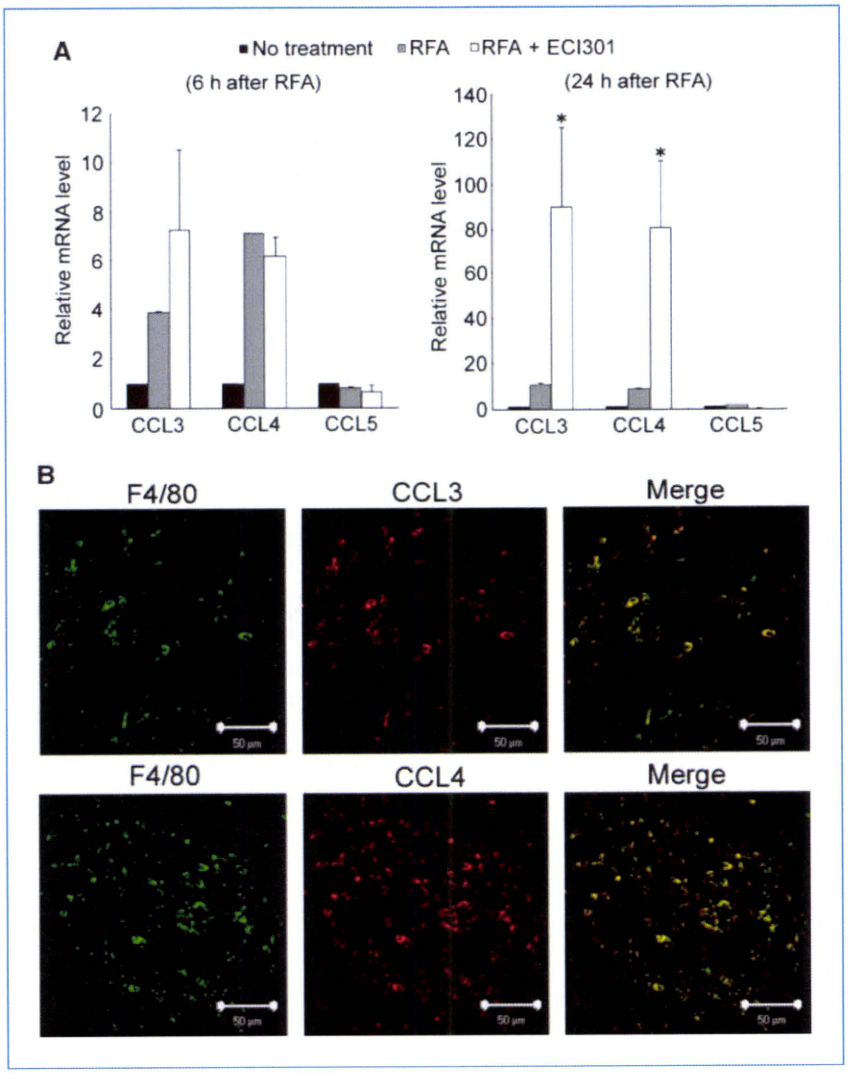

Figure 5. Increased CCL3 expression in RFA-treated tumors. A, real-time RT-PCR was performed on total RNA extracted from RFA-treated tumors of WT mice. The tumors were harvested 6 h (left) or 24 h (right) after RFA. Chemokine mRNA levels were normalized to GAPDH mRNA levels. Columns, mean (n = 3); bars, SD. *, $P < 0.05$, compared with untreated mice. B, RFA-treated tumors were removed from WT mice on day 1 after RFA plus ECI301 treatment and immunostained with the indicated combinations of antibodies as described in Materials and Methods. Right, digitally merged images. Representative results from three individual animals. Original magnification, ×400. Bar, 50 μm.

On the contrary, administration of ECI301 without RFA did not result in a significant decrease in tumor size (Fig. 1C). These observations suggest that ECI301 can augment RFA-induced antitumor effects but fails to induce antitumor effects by itself.

Deficiency of *CCR1* abrogates increased antitumor effect of ECI301 after RFA

ECI301 uses two distinct chemokine receptors, CCR1 and CCR5. To elucidate the roles of these chemokine receptors, either tumor-bearing *CCR1*$^{-/-}$ or *CCR5*$^{-/-}$ mice were similarly treated with RFA plus ECI301. RFA retarded the growth of non–RFA-treated tumors in *CCR1*$^{-/-}$ mice similar to that in WT mice, but ECI301 failed to further accentuate RFA-induced growth retardation of non–RFA-treated tumors (Fig. 2A). In contrast, ECI301 augmented RFA-mediated inhibition of non–RFA-treated tumors in *CCR5*$^{-/-}$ mice, resulting in complete tumor eradication in one of six mice (Fig. 2B). These observations indicate that CCR1-expressing, but not CCR5-expressing, cells play an important role in ECI301-induced augmentation of tumor regression after RFA.

ECI301 increases CCR1-expressing cells in peripheral blood and RFA-treated tumors after RFA

The reported capacity of CCL3 to mobilize leukocytes into peripheral blood (15, 16) prompted the investigation of the

Figure 4. ECI301 increases infiltration of CCR1-expressing leukocytes into RFA-treated tumors after RFA. RFA-treated tumors were removed from WT or *CCR1*$^{-/-}$ mice 8 h after RFA. A, B, and D, immunohistochemical analysis was performed using anti-CD4, anti-CD8a, anti-CD11c, or anti-F4/80 antibodies. A, representative results from three individual WT mice in each group. Original magnification, ×400. Bar, 50 μm. B and D, the numbers of CD4$^+$, or CD8$^+$, CD11c$^+$, or F4/80$^+$ cells were counted. Cell density was determined in 10 randomly chosen tumor areas at 400-fold magnification. Columns, mean (n = 5); bars, SD. **, $P < 0.01$. C, RFA-treated tumor tissues were processed using double-color immunofluorescence analysis as described in Materials and Methods. Right, digitally merged images. Representative results from three individual animals. Original magnification, ×400. Bar, 50 μm.

Published OnlineFirst July 27, 2010; DOI:10.1158/0008-5472.CAN-10-0096

effects of ECI301 on peripheral blood. RFA alone had few effects on the numbers of CCR1-expressing cells, but subsequent ECI301 administration increased the numbers of CCR1-expressing cells in peripheral blood, particularly $CD11c^+$ cells, but not $CD4^+$ or $CD8^+$ cells (Fig. 3). Because immune cells need to accumulate in RFA-treated tumors at an early stage to initiate adaptive immune responses, CCR1 expression by tumor-infiltrating cells in RFA-treated tumors was examined 8 hours after treatment. RFA-induced $CD4^+$, $CD8^+$, $CD11c^+$, and $F4/80^+$ cell infiltrations into RFA-treated tumors were greater than those into tumors of untreated mice. Moreover, ECI301 further increased the numbers of $CD4^+$, $CD8^+$, and $CD11c^+$ cells infiltrating into RFA-treated tumors compared with the numbers of these cells infiltrating into tumors treated with RFA alone (Fig. 4A and B). In RFA-treated tumors, most $CD11c^+$ and $F4/80^+$ cells expressed CCR1, whereas few $CD4^+$ and $CD8^+$ cells expressed CCR1 (Fig. 4C). Furthermore, ECI301-induced $CD4^+$, $CD8^+$, and

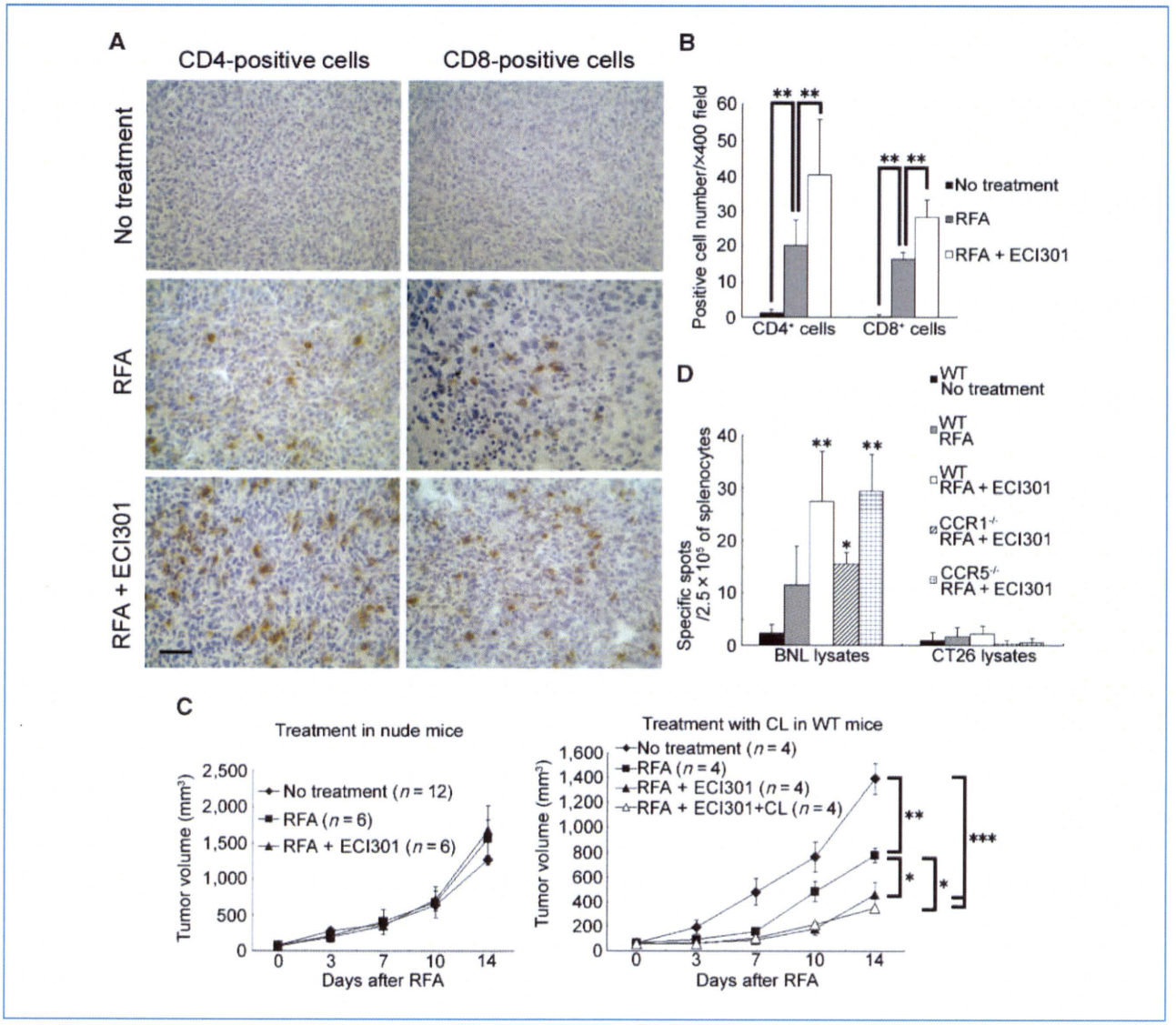

Figure 6. ECI301 augments tumor-specific immune responses after RFA. A, non–RFA-treated tumors were removed from WT mice on day 3 after RFA, and immunohistochemical analysis was done using anti-CD4 or anti-CD8a antibodies. Representative results from three individual animals in each group. Original magnification, ×400. Bar, 50 μm. B, the numbers of $CD4^+$ or $CD8^+$ cells were counted. Cell density was determined in 10 randomly chosen tumor areas at 400-fold magnification. Columns, mean (n = 5); bars, SE. **, $P < 0.01$. C, BALB/c-*nu/nu* mice (left) and BALB/c-WT mice (right) were inoculated with BNL cells and treated as described in the legend to Fig. 1. In the RFA + ECI301 + clodronate liposome (CL) group, the mice were injected with 200 μL of CL to deplete monocytes/macrophages as described in Materials and Methods. Non–RFA-treated tumor volumes were measured twice a week. Points, mean; bars, SE. D, spleens from WT, *CCR1*$^{-/-}$, or *CCR5*$^{-/-}$ mice were harvested on day 21 after RFA, and mononuclear cells were separated from the spleens for ELISPOT assay as described in Materials and Methods. The number of specific spots was determined by subtracting the number of spots in wells without lysates from the number of spots in wells with tumor lysates. Columns, mean (n = 3); bars, SE. *, $P < 0.05$; **, $P < 0.01$, compared with untreated WT mice.

Published OnlineFirst July 27, 2010; DOI:10.1158/0008-5472.CAN-10-0096

CD11c$^+$ cell infiltrations into ablated tumors were lesser in *CCR1*$^{-/-}$ mice than in WT mice, whereas F4/80$^+$ cells infiltrated RFA-treated tumors in *CCR1*$^{-/-}$ mice and WT mice to a similar extent (Fig. 4D). These observations suggest that ECI301 augments RFA-induced CD4$^+$, CD8$^+$, and CD11c$^+$ cell infiltrations into RFA-treated tumors in a CCR1-dependent manner.

ECI301 increases intratumoral expression of CCL3 after RFA

We showed that CCR1$^+$ cells were mobilized into blood by i.v. administered ECI301. However, the concentration of ECI301 in blood can go down rapidly as time passes (the peak is 5 minutes, and the half-life is <2 hours),[4] allowing ECI301-mobilized CCR1$^+$ cells to migrate into tissues where chemokines are highly produced. To prove this point, chemokine expression in RFA-treated tumors was examined. RFA plus ECI301 treatment increased *CCL3* mRNA expression level 6 hours after RFA. Moreover, 24 hours after treatment, *CCL3* and *CCL4* mRNA expression levels became almost 10-fold higher in tumors treated with RFA alone than in tumors of untreated mice, and ECI301 further increased the mRNA expression level of these chemokines in RFA-treated tumors (Fig. 5A). CCL3 and CCL4 were detected in tumor-infiltrating F4/80$^+$ cells (Fig. 5B). These observations indicate that RFA treatment causes local production of CCL3 and CCL4 in RFA-treated tumors and ECI301 further increases the expression of these chemokines. As the concentration of ECI301 in blood decreases, chemokines produced locally in RFA-treated tumor can attract CCR1-expressing CD11c$^+$ cells, thereby indirectly inducing CCR1-negative CD4$^+$ and CD8$^+$ cell infiltrations.

ECI301 augments RFA-induced tumor-specific immune responses accompanied by T-cell infiltrations into non–RFA-treated tumors

Non–RFA-treated tumors were analyzed histologically to clarify the mechanisms underlying the CCR1-dependent inhibitory effect of RFA plus ECI301 treatment against these tumors. Although few CD4$^+$ or CD8$^+$ cells were observed in the tumors of untreated mice, RFA treatment increased the numbers of CD4$^+$ and CD8$^+$ cells in the non–RFA-treated tumors 3 days after RFA. ECI301 further augmented RFA-induced CD4$^+$ and CD8$^+$ cell infiltrations into non–RFA-treated tumors (Fig. 6A and B). However, only a marginal number of CD11c$^+$ or F4/80$^+$ cells infiltrated into non–RFA-treated tumors of mice treated with RFA alone or RFA plus ECI301-treated mice (data not shown). Based on these findings, we hypothesized that ECI301-augmented tumor regression after RFA may be associated with T-cell–mediated antitumor immune responses. To clarify this point, *nu/nu* mice on a BALB/c background were treated by RFA with or without ECI301. Deficiency of T cells abrogated the tumor-inhibitory effect of ECI301 as well as the RFA-induced antitumor effect (Fig. 6C). Thus, both ECI301- and RFA-induced tumor regressions require T-cell–mediated antitumor immune response.

[4] Unpublished data from Effector Cell Institute.

However, CD4$^+$ or CD8$^+$ T cells rarely expressed CCR1 in blood and RFA-treated tumors. CCR1$^+$ cells in RFA-treated tumors were CD11c$^+$ cells and F4/80$^+$ cells, and only the former accumulate in RFA-treated tumors in a CCR1-dependent manner. These findings suggest that CCR1-positive CD11c$^+$ cells may activate antitumor T-cell responses and indirectly induce tumor retardation. Accordingly, we next examined the effect of depletion of monocytes/macrophages on ECI301-augmented tumor regression. I.p. injection of clodronate liposome depleted CD11c-negative monocytes in blood, although it did not change the number of CD11c$^+$ cells (data not shown). Depletion of these CD11c-negative monocytes did not cause any effects on ECI301-enhanced tumor regression, indicating that ECI301-augmented antitumor T-cell immunity was independent of CD11c-negative monocytes (Fig. 6C).

Finally, to prove the presence of systemic adaptive immune responses, IFN-γ ELISPOT assay was performed using mononuclear cells from the spleen. A greater number of spots against BNL cell lysates, but not against CT26 cell lysates, were generated by RFA plus ECI301–treated mice than that by mice treated with RFA alone or untreated mice. Moreover, ablation of *CCR1* gene, but not *CCR5* gene, reduced the number of spots against BNL cell lysates even when the mice were treated with RFA plus ECI301 (Fig. 6D). These observations suggest that ECI301 can further augment RFA-induced tumor-specific adaptive immune responses and subsequent tumor retardation in a CCR1-dependent manner.

Discussion

HCC occurs predominantly in individuals with chronic liver disease related to hepatitis B or hepatitis C virus infections (22–24). In addition to surgical resection, RFA treatment has been developed to eradicate solitary HCC lesions (25). RFA of HCC induces specific T-cell responses against liver tumors in human and rabbit (8, 11). Moreover, activated dendritic cells were detected in peripheral blood of HCC patients after RFA (9). These previous reports indicate that RFA treatment can induce antitumor immune responses against HCC (8–11). Likewise, we observed that RFA treatment generated tumor-specific IFN-γ–producing cells and inhibited the growth of non–RFA-treated tumors accompanied by massive T-cell infiltration into these tumors. However, even after successful ablation of HCC lesion by RFA, tumor recurrence often occurs probably because HCC develops in a multicentric manner in the cirrhotic liver (12). These observations indicate that RFA-induced augmentation in immune response may not be sufficient to prevent tumor recurrence. Thus, a novel therapeutic modality is required to further augment RFA-induced tumor-specific immune responses. Here, we showed that combined administration of ECI301 and RFA can augment tumor-specific immune responses against HCC.

Several chemokines are used for immunotherapy against cancers because they can attract immune cells such as dendritic and cytotoxic T cells to augment tumor-specific immune responses (26). However, some chemokines can simultaneously attract myeloid-derived suppressor and regulatory T cells to promote neovascularization and induce immunosuppressive

Published OnlineFirst July 27, 2010; DOI:10.1158/0008-5472.CAN-10-0096

microenvironments (26–28). The double-edged activities of chemokines frequently preclude their use for tumor immunotherapy. Moreover, most chemokines exhibit a bell-shaped dose-response curve with a narrow effective dose window. Thus, determination of an optimal dose of chemokines is important to elicit efficient antitumor responses (29). Several lines of evidence show that intratumoral use of CCL3 reduces tumorigenicity (6, 30). Furthermore, there are no reports showing that use of CCL3 can promote tumor progression. We observed that systemic administration of ECI301 without RFA treatment induced neither reduction nor progression of tumors. On the contrary, systemic injection of ECI301 after RFA can inhibit the growth of non–RFA-treated tumors in the contralateral side. ECI301-enhanced tumor regression after RFA was both CCR1 and T-cell dependent, but T cells rarely expressed CCR1 in blood and RFA-treated tumors. Because depletion of monocytes/macrophages did not affect the retardation of ECI301-treated tumors, CCR1-expressing $CD11c^+$ dendritic cells might activate antitumor T-cell responses and indirectly induce tumor retardation via some mechanisms such as antigen presentation and cytokine production. ECI301 mobilized a large number of $CCR1^+$ cells into blood, and these mobilized cells may be attracted into highly CCL3-producing RFA-treated tumors and cause increased number of tumor-infiltrating $CCR1^+CD11c^+$ dendritic cells. Thus, $CCR1^+$ precursors in blood and $CCR1^+CD11c^+$ tumor-infiltrating dendritic cells might play important roles in ECI301-augmented antitumor effects (31–33).

ECI301 could not increase the number of $F4/80^+$ cells in the RFA-treated tumor sites. Accumulation of $F4/80^+$ cells in the tumor treated with ECI301 plus RFA was also independent of CCR1. $F4/80^+$ cells, which might include a large number of macrophages/monocytes, are usually attracted into the tumor by CCL2, CCL4, and CCL5 that are produced in the tumor sites. CCR2, the receptor for CCL2, and CCR5, the receptor for CCL4 and CCL5, might be responsible for migration of monocytes/macrophages (27, 34–36). However, it is still unclear whether monocytes/macrophages use CCR2 or CCR5 after massive tumor cell death caused by treatments such as RFA because tumor cell death induces different profiles of chemokine production in the tumors (4). Although ECI301 did not directly induce migration of $F4/80^+$ cells, the mechanism underlying the infiltration of $F4/80^+$ macrophages remains to be elucidated.

Breaking tolerance for tumor cells is necessary for induction of antitumor immunity. Several independent groups have suggested multiple mechanisms underlying immunogenic tumor cell death induced by anticancer chemotherapy or radiation therapy (37–40). Anthracyclin causes apoptosis along with translocation of calreticulin to the apoptotic tumor cell surface. Calreticulin exposure augments phagocytosis of apoptotic cancer cells by dendritic cells with an eventual increase in immune response (37, 38). Chemotherapy or irradiation kills tumor cells to release high mobility group box 1 (HMGB1). Released HMGB1 activates dendritic cells after binding to toll-like receptor 4 expressed by these cells (39). Apoptosis induced by local radiation therapy augments MHC class I expression by tumor cells, thereby facilitating their recognition by cytotoxic T cells (40). RFA induces the expression of heat shock proteins 70 and 90 on ablated tumor cells, and these proteins can activate toll-like receptor–expressing antigen-presenting cells (41, 42). In addition, we showed that RFA treatment alone caused local production of CCL3 in RFA-treated tumors accompanied by accumulation of T cells and $CD11c^+$ dendritic cells. These mechanisms may also account for the observed RFA-induced generation of tumor-specific immune responses.

We revealed that combined treatment of ECI301 and RFA augmented antitumor-specific immune responses, thereby inhibiting the growth of non–RFA-treated tumors in a CCR1-dependent manner. Thus, combined treatment of ECI301 and RFA can prevent human HCC from recurring after RFA treatment. The absence of any severe adverse effects in mice (data not shown) further warrants the clinical trial of ECI301 combined with RFA as a treatment regimen for HCC.

Disclosure of Potential Conflicts of Interest

No potential conflicts of interest were disclosed.

Acknowledgments

We thank Dr. Philip M. Murphy (National Institute of Allergy and Infectious Disease, NIH) and Dr. Kouji Matsushima (Tokyo University) for providing us with $CCR1^{-/-}$ and $CCR5^{-/-}$ mice, respectively.

The costs of publication of this article were defrayed in part by the payment of page charges. This article must therefore be hereby marked *advertisement* in accordance with 18 U.S.C. Section 1734 solely to indicate this fact.

Received 01/11/2010; revised 06/01/2010; accepted 06/20/2010; published OnlineFirst 07/27/2010.

References

1. Luster AD. Chemokines—chemotactic cytokines that mediate inflammation. N Engl J Med 1998;338:436–45.
2. Castellino F, Huang AY, Altan-Bonnet G, Stoll S, Scheinecker C, Germain RN. Chemokines enhance immunity by guiding naïve $CD8^+$ T cells to sites of $CD4^+$ T cell-dendritic cell interaction. Nature 2006;440:890–5.
3. Sozzani S. Dendritic cell trafficking: more than just chemokines. Cytokine Growth Factor Rev 2005;16:581–92.
4. Iida N, Nakamoto Y, Baba T, et al. Tumor cell apoptosis induces tumor-specific immunity in a CC chemokine receptor 1-and 5-dependent manner in mice. J Leukoc Biol 2008;84:1001–10.
5. Tsuchiyama T, Nakamoto Y, Sakai Y, et al. Prolonged, NK cell-mediated antitumor effects of suicide gene therapy combined with monocyte chemoattractant protein-1 against hepatocellular carcinoma. J Immunol 2007;178:574–83.
6. Crittenden M, Gough M, Harrington K, Olivier K, Thompson J, Vile RG. Expression of inflammatory chemokines combined with local tumor destruction enhances tumor regression and long-term immunity. Cancer Res 2003;63:5505–12.
7. Furumoto K, Soares L, Engleman EG, Merad M. Induction of potent antitumor immunity by *in situ* targeting of intratumoral DCs. J Clin Invest 2004;113:774–83.

Published OnlineFirst July 27, 2010; DOI:10.1158/0008-5472.CAN-10-0096

8. Zerbini A, Pilli M, Penna A, et al. Radiofrequency thermal ablation of hepatocellular carcinoma liver nodules can activate and enhance tumor-specific T-cell responses. Cancer Res 2006;66:1139–46.
9. Ali MY, Grimm CF, Ritter M, et al. Activation of dendritic cells by local ablation of hepatocellular carcinoma. J Hepatol 2005;43:817–22.
10. Brok MH, Sutmuller RP, Voort R, et al. *In situ* tumor ablation creates antigen source for the generation of antitumor immunity. Cancer Res 2004;64:4024–9.
11. Wissniowski TT, Hünsler J, Neureiter D, et al. Activation of tumor-specific T lymphocytes by radio-frequency ablation of the VX2 hepatoma in rabbits. Cancer Res 2003;63:6496–500.
12. Poon RT, Fan ST, Ng IO, Lo CM, Liu CL, Wong J. Different risk factors and prognosis for early and late intrahepatic recurrence after resection of hepatocellular carcinoma. Cancer 2000;89:500–7.
13. Hunter MG, Bawden L, Brotherton D, et al. BB-10010: an active variant of human macrophage inflammatory protein-1α with improved pharmaceutical properties. Blood 1995;86:4400–8.
14. Clemons MJ, Marshall E, Dürig J, et al. A randomized phase-II study of BB-10010 (macrophage inflammatory protein-1α) in patients with advanced breast cancer receiving 5-fluorouracil, Adriamycin, and cyclophosphamide chemotherapy. Blood 1998;92:1532–40.
15. Zhang Y, Yoneyama H, Wang Y, et al. Mobilization of dendritic cell precursors into the circulation by administration of MIP-1α in mice. J Natl Cancer Inst 2004;96:201–9.
16. Taub DD, Conlon K, Lloyd AR, Oppenheim JJ, Kelvin DJ. Preferential migration of activated $CD4^+$ and $CD8^+$ T cells in response to MIP-1α and MIP-1β. Science 1993;260:355–8.
17. Shiraishi K, Ishiwata Y, Nakagawa K, et al. Enhancement of antitumor radiation efficacy and consistent induction of the abscopal effect in mice by ECI301, an active variant of macrophage inflammatory protein-1α. Clin Cancer Res 2008;14:1159–66.
18. Isoai A, Kimura H, Reichert A, et al. Production of D-amino acid oxidase of *Trigonopsis variabilis* in *Schizosaccharomyces pombe* and the characterization of biocatalysts prepared with recombinant cells. Biotechnol Bioeng 2002;80:22–32.
19. Lu P, Nakamoto Y, Nemoto-Sakai Y, et al. Potential interaction between CCR1 and its ligand, CCL3, induced by endogeneously produced interleukin-1 in human hepatomas. Am J Pathol 2003;162:1249–58.
20. Lu P, Li L, Liu G, Rooijen N, Mukaida N, Zhang X. Opposite roles of CCR2 and CX3CR1 macrophages in alkali-induced corneal neovascularization. Cornea 2009;28:562–9.
21. Sadahira Y, Yasuda T, Yoshino T, et al. Impaired splenic erythropoiesis in phlebotomized mice injected with CL2MDP-liposome: an experimental model for studying the role of stromal macrophages in erythropoiesis. J Leukoc Biol 2000;68:464–70.
22. Tsukuma H, Hiyama T, Tanaka S, et al. Risk factors for hepatocellular carcinoma among patients with chronic liver disease. N Engl J Med 1993;328:1797–801.
23. Velázquez RF, Rodríguez M, Navascués CA, et al. Prospective analysis of risk factors for hepatocellular carcinoma in patients with liver cirrhosis. Hepatology 2003;37:520–7.
24. Okita K. Management of hepatocellular carcinoma in Japan. J Gastroenterol 2006;41:100–6.
25. Tateishi R, Shiina S, Ohki T, et al. Treatment strategy for hepatocellular carcinoma: expanding the indication for radiofrequency ablation. J Gastroenterol 2009;44 Suppl:142–6.
26. Homey B, Müller A, Zlotnik A. Chemokines: agents for the immunotherapy of cancer? Nat Rev Immnol 2002;2:175–84.
27. Balkwill F. Cancer and the chemokine network. Nat Rev Cancer 2004;4:540–50.
28. Dell'Agnola C, Biragyn A. Clinical utilization of chemokines to combat cancer: the double-edged sword. Expert Rev Vaccines 2007;6:267–83.
29. Tsuchiyama T, Nakamoto Y, Sakai Y, Mukaida N, Kaneko S. Optimal amount of monocyte chemoattractant protein-1 enhances antitumor effects of suicide gene therapy against hepatocellular carcinoma by M1 macrophage activation. Cancer Sci 2008;99:2075–82.
30. Nakashima E, Ova A, Kubota YA. A candidate for cancer gene therapy: MIP-1α gene transfer to an adenocarcinoma cell line reduced tumorigenesity and induced protective immunity in immunocompetent mice. Pharm Res 1996;13:1896–901.
31. Geissmann F, Manz MG, Jung S, Sieweke MH, Merad M, Ley K. Development of monocytes, macrophages, and dendritic cells. Science 2010;327:656–61.
32. Randolph GJ, Ochando J, Partida-Sánchez S. Migration of dendritic cell subsets and their precursors. Annu Rev Immunol 2008;26:293–316.
33. López-Bravo M, Ardavín C. *In vivo* induction of immune responses to pathogens by conventional dendritic cells. Immunity 2008;29:343–51.
34. Murdoch C, Muthana M, Coffelt SB, Lewis CE. The role of myeloid cells in the promotion of tumor angiogenesis. Nat Rev Cancer 2008;8:618–31.
35. Azenshtein E, Luboshits G, Shina S, et al. The CC chemokine RANTES in breast carcinoma progression: regulation of expression and potential mechanism of promalignant activity. Cancer Res 2002;62:1093–102.
36. Nesbit M, Schaider H, Miller TH, Herlyn M. Low-level monocyte chemoattractant protein-1 stimulation of monocytes leads to tumor formation in nontumorigenic melanoma cells. J Immunol 2001;166:6483–90.
37. Obeid M, Tesniere A, Ghiringhelli F, et al. Calreticulin exposure dictates the immunogenicity of cancer cell death. Nat Med 2007;13:54–61.
38. Casares N, Pequignot MO, Tesniere A, et al. Caspase-dependent immunogenicity of doxorubicin-induced tumor cell death. J Exp Med 2005;202:1691–701.
39. Apetoh L, Ghiringhelli F, Tesniere A, et al. Toll-like receptor 4-dependent contribution of the immune system to anticancer chemotherapy and radiotherapy. Nat Med 2007;13:1050–9.
40. Reits EA, Hodge JW, Herberts CA, et al. Radiation modulates the peptide repertoire, enhances MHC class I expression, and induces successful antitumor immunotherapy. J Exp Med 2006;203:1259–71.
41. Schueller G, Kettenbach J, Sedivy R, et al. Heat shock protein expression induced by percutaneous radiofrequency ablation of hepatocellular carcinoma *in vivo*. Int J Oncol 2004;24:609–13.
42. Nikfarjam M, Muralidharan V, Su K, Malcontenti-Wilson C, Christophi C. Patterns of heat shock protein (HSP70) expression and Kupffer cell activity following thermal ablation of liver and colorectal liver metastasis. Int J Hyperthermia 2005;21:319–32.

THE JOURNAL OF GENE MEDICINE
J Gene Med 2010;**12**: 1002–1013.
Published online in Wiley Online Library (wileyonlinelibrary.com) **DOI:** 10.1002/jgm.1528

RESEARCH ARTICLE

Prevention of intrahepatic metastasis of liver cancer by suicide gene therapy and chemokine ligand 2/monocyte chemoattractant protein-1 delivery in mice

Kaheita Kakinoki[1]
Yasunari Nakamoto[1]
Takashi Kagaya[1]
Tomoya Tsuchiyama[1]
Yoshio Sakai[1]
Tohru Nakahama[1]
Naofumi Mukaida[2]
Shuichi Kaneko[1]*

[1]*Disease Control and Homeostasis, Graduate School of Medical Science, Kanazawa University, Kanazawa, Japan*

[2]*Division of Molecular Bioregulation, Cancer Research Institute, Kanazawa University, Kanazawa, Japan*

*Correspondence to:
Shuichi Kaneko, Disease Control and Homeostasis, Graduate School of Medical Science, Kanazawa University, 13-1 Takara-machi, Kanazawa 920-8641, Japan
E-mail: skaneko@m-kanazawa.jp

Received: 22 June 2010
Revised: 28 October 2010
Accepted: 5 November 2010

Abstract

Background The prognosis of patients with hepatocellular carcinoma (HCC) remains poor, largely as a result of intrahepatic metastasis. Using a mouse model of intrahepatic metastasis, we investigated whether chemokine ligand 2/monocyte chemoattractant protein-1 (CCL2/MCP-1) could potentiate the antitumor effects of the herpes simplex virus thymidine kinase/ganciclovir (HSV-tk/GCV) system.

Methods Mouse hepatoma cells infected with recombinant adenovirus vectors expressing HSV-tk, CCL2/MCP-1 and LacZ at multiplicities of infection of Ad-tk/Ad-MCP1 = 3/0.03 (T/M^{Low}), 3/3 (T/M^{High}) and Ad-tk/Ad-LacZ = 3/3 (T/L) were injected into BALB/c mice.

Results Intrahepatic tumor growth was significantly lower in T/M^{Low} mice. By contrast, no tumor suppression was observed in T/M^{High} mice. The tumor-specific cytolytic activities of splenocytes from T/M^{Low} and T/M^{High} mice were comparable. Immunohistochemical analysis of liver tissues showed similar infiltration by Mac-1^+ and T cells in these animals, whereas the proportions of classical activated (M1) monocytes/macrophages were significantly higher in T/M^{Low} mice. In addition, interleukin-12 production was elevated in these tissues. Vascular endothelial growth factor-A expression and $CD31^+$ microvessels were increased in T/M^{High} mice.

Conclusions Collectively, these results demonstrate that an adequate amount of CCL2/MCP-1, together with the HSV-tk/GCV system, may induce T helper 1-polarized antitumor effects without inducing tumor angiogenesis in the microenvironment of intrahepatic HCC progression. Copyright © 2010 John Wiley & Sons, Ltd.

Keywords chemokines; hepatocellular carcinoma; monocytes/macrophages

Introduction

Primary liver cancer is the fifth most common neoplasm in the world and the third most common cause of cancer-related deaths [1,2]. Despite the development of novel modalities for the treatment of hepatocellular carcinoma (HCC), including transcatheter arterial embolization, percutaneous ablation, surgical resection and liver transplantation, the prognosis of patients with HCC still remains relatively poor. One of the major factors responsible for

these unsatisfactory outcomes is the high frequency of intrahepatic recurrence after curative treatment [1,2]. Intrahepatic recurrence is the result of two mechanisms: intrahepatic metastasis (IM) originating from the primary cancer, and a second primary cancer arising from multicentric carcinogenesis (MC). IM may correlate with early recurrence and poor prognosis, whereas MC is associated with relatively good prognosis [3–5].

To develop novel antitumor strategies for HCC, we have investigated the effectiveness of immune gene therapy using suicide genes and chemokine molecules, including chemokine ligand 2/monocyte chemoattractant protein-1 (CCL2/MCP-1) [6–8]. CCL2/MCP-1 is a chemokine that regulates the recruitment of monocytes/macrophages to inflammatory sites and tumor tissues, as well as their activation, including lysosomal enzyme release and tumoricidal activity, and is functional in both mice and humans [9]. Transfectant-derived CCL2/MCP-1 has been found to successfully recruit monocytes into tumor tissue [10,11]. We recently described a combination strategy for the treatment of HCC, consisting of the herpes simplex virus thymidine kinase/ganciclovir (HSV-tk/GCV) system and CCL2/MCP-1 gene delivery. We found that adenovirally delivered CCL2/MCP-1 enhanced the antitumor effects of the HSV-tk/GCV system by activating innate immune responses involving monocytes/macrophages, as well as demonstrating prolonged efficacy mediated by natural killer cells [6–8]. These experiments were performed in athymic nude mice, deficient in acquired immune responses, subcutaneously transplanted with HCC.

In the present study, we have used a liver metastasis model, in which tumor cells were infused through the portal vein (PV), to investigate whether CCL2/MCP-1 gene delivery could potentiate the antitumor effects of the suicide gene system. The results obtained indicate that the antitumor effects of the suicide gene are enhanced by codelivery of an adequate amount of CCL2/MCP-1. These antitumor effects were associated with the recruitment of monocytes/macrophages and T cells, T helper 1 (Th1) cytokine gene expression and the induction of splenocyte cytolytic activity. These findings indicate that CCL2/MCP-1 has an immunomodulatory effect on suicide gene therapy for HCC by orchestrating the innate and acquired immune responses.

Materials and methods

Animals

Male BALB/cA Jcl mice, 6–8 weeks of age, were obtained from CLEA Japan Inc. (Tokyo, Japan), maintained at constant room temperature (25 °C) and provided with free access to standard diet and tap water throughout, in accordance with institutional guidelines.

Cell lines and cell culture

The mouse HCC cell line BNL 1ME A.7R.1 (BNL) and the mouse colon cancer cell line colon 26 clone 20 (CT 26), derived from BALB/c mice (H-2d), were cultured in Dulbecco's modified Eagle's medium supplemented with 10% heat-inactivated (30 min at 56 °C) fetal bovine serum (FBS), non-essential amino acids, sodium pyruvate, HEPES buffer, 2 mM glutamate, 1 mM penicillin/streptomycin and 0.2 mM gentamicin (Gibco, Long Island, NY, USA) at 37 °C in 5% CO_2.

Recombinant adenovirus vectors

The following replication-defective adenovirus vectors, driven by the CAG promoter [12], were prepared by recombinant DNA technology: Ad-tk, which expresses the HSV-tk gene; Ad-MCP1, which expresses the human CCL2/MCP-1 gene; and Ad-LacZ, which expresses the LacZ gene [13] (Figure 1A). Each recombinant adenovirus vector was purified and titered according to protocols supplied by the manufacturer (Takara, Ootsu, Japan). Briefly, each gene fragment (i.e. HSV-tk, CCL2/MCP-1 and LacZ) was excised from its respective insert-containing pBluescript vector and inserted into the cosmid pAxCA-wt (Takara, Ootsu, Japan), which contains essentially the full-length adenovirus type 5 genome apart from the E1 and E3 regions, thus generating the pAxCA gene (Figure 1A). The recombinant adenovirus vectors (rAds) were generated by transfecting 293 cells with pAxCA-gene and adenovirus 5-dIX DNA-terminal protein complex. These rAds were propagated in 293 cells [14], and viral stocks were prepared by standard protocols [15]. The titers of rAds were determined by the 50% tissue culture infectious dose ($TCID_{50}$) method [16].

Enzyme-linked immunosorbent assay (ELISA) for CCL2/MCP-1

Aliquots of 2.5×10^4 BNL cells were seeded in 3.0 ml of culture media in six-well tissue culture plate. After 24 h, the cells were infected with Ad-MCP1 and Ad-MCP1, together with Ad-tk, at various multiplicities of infections (MOIs). After 24 h, the media were collected from the wells, and the concentrations of CCL2/MCP-1 were determined by ELISA. Briefly, each well of a 96-well microtiter plate (Nalgene, Rochester, NY, USA) was coated with 0.05 M carbonate buffer (pH 9.6) containing monoclonal anti-human CCL2/MCP-1 antibody (ME 6.1; 1 μg/ml) overnight at 4 °C. After washing with phosphate-buffered saline (PBS) containing 0.05% Tween 20, the plates were blocked with PBS containing 1% bovine serum albumin for 1 h at 37 °C. Diluted culture medium or various concentrations of recombinant CCL2/MCP-1 were added to duplicate wells and incubated for 2 h at 37 °C. The plates were washed, incubated with rabbit anti-CCL2/MCP-1 antibodies (1 μg/ml) for 2 h at 37 °C,

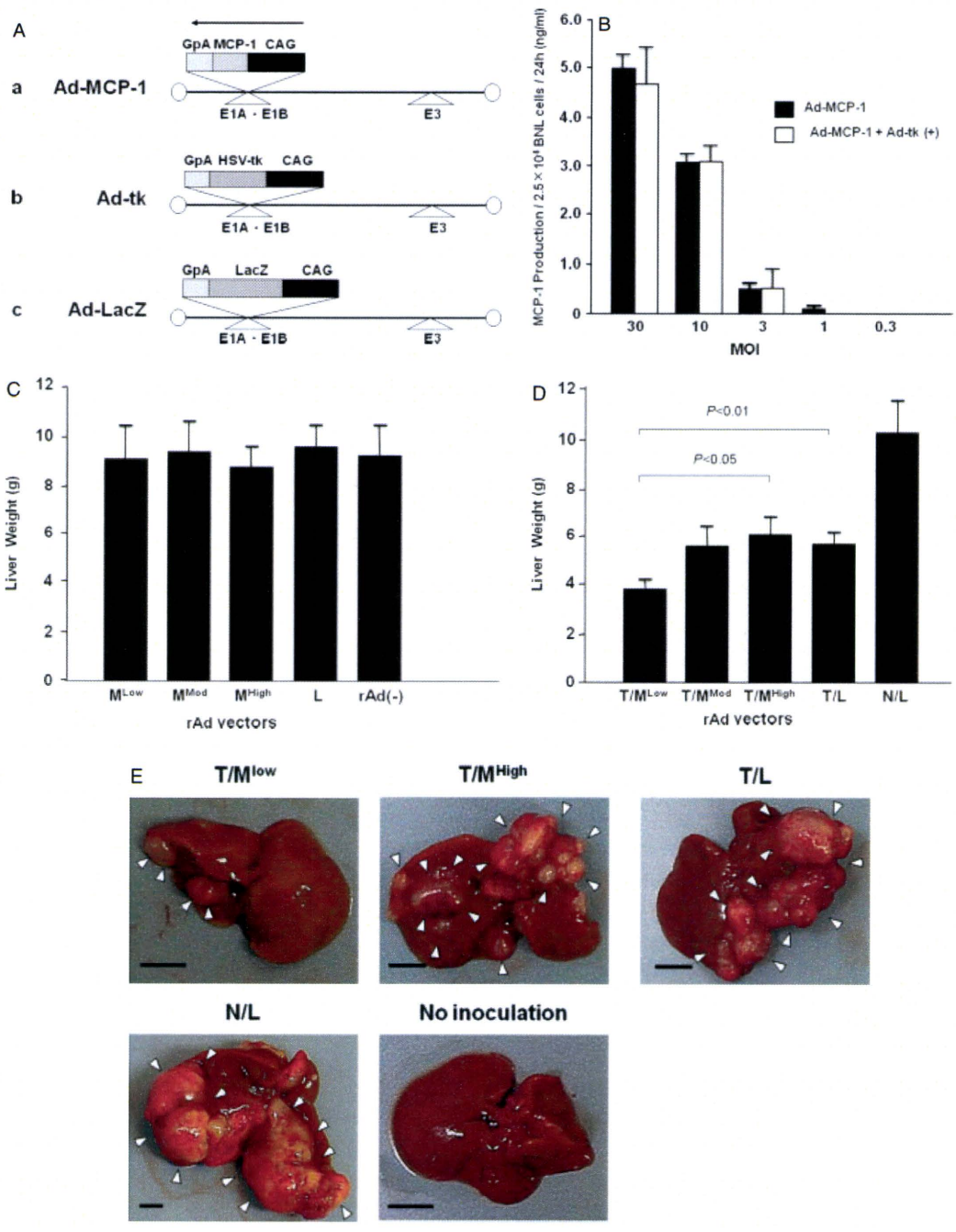

Figure 1. CCL2/MCP-1 production and antitumor effects of rAds. (A) Schematic representation of rAds expressing each gene under the control of a CAG promoter. (a) Ad-MCP1 expressing CCL2/MCP-1. (b) Ad-tk expressing HSV-tk. (c) Ad-LacZ expressing β-galactosidase gene (LacZ). Solid lines indicate the rAd genome, and the open triangle below each rAd genome represents the deletion of adenovirus early regions. The arrow shows the orientation of transcription. GpA, rabbit β-globin (A) site; CAG, CAG promoter. (B) Production of CCL2/MCP-1 by BNL cells infected with rAds at various MOIs. The CCL2/MCP-1 concentrations in culture supernatants were determined by ELISA. Data shown are the mean ± SE of three independent results. (C) Liver weight following transfer of BNL cells infected with Ad-MCP1, Ad-LacZ or PBS (–). Each mouse was injected via the PV with 1×10^6 BNL cells infected with Ad-MCP1 at various MOIs: 0.03 (M^{Low}), 0.3 (M^{Mod}) and 3 (M^{High}), and Ad-LacZ at the MOI of 3 (L), and the whole livers were weighed on day 21. (D) CCL2/MCP-1 enhancement of the antitumor effects of the HSV-tk/GCV system against intrahepatic cancer cells. Each mouse was injected via the PV with BNL cells (1×10^6) infected with Ad-tk, Ad-MCP1 and Ad-LacZ at various MOIs: Ad-tk/Ad-MCP1 = 3/0.03 (T/M^{Low}), 3/0.3 (T/M^{Mod}) and 3/3 (T/M^{High}); Ad-tk/Ad-LacZ = 3/3 (T/L); and Ad-LacZ = 6 (N/L), and the whole livers were weighed on day 21. (E) The macroscopic views of hepatic tumors (open arrowheads) in mice. Tumor growth was markedly suppressed in T/M^{Low} mice. Scale bars = 10 mm

DOI: 10.1002/jgm

washed again and incubated with alkaline phosphatase-conjugated goat anti-rabbit antibody (1:12 000; Tago, Burlingame, CA, USA) for 2 h at 37 °C. The plates were washed, aliquots of 1 mg/ml *p*-nitrophenylphosphate (Sigma, St Louis, MO, USA) in 1 M diethanolamine (pH 9.8) supplemented with 0.5 mM $MgCl_2$ were added to the wells, and the plates were incubated for 40 min at room temperature. After addition of 1 M NaCl, the optical density (at 405 nm) was assessed using an ELISA plate reader (MTP-120; Corona Electric, Ibaragi, Japan). All experiments were repeated in triplicate.

Disease model

To evaluate the direct antitumor effect of CCL2/MCP-1, 1×10^7 BNL cells suspended in 0.5 ml of culture medium were infected *in vitro* with CCL2/MCP-1 at various MOIs: 0.03 (M^{Low}), 0.3 (M^{Mod}) and 3 (M^{High}); Ad-LacZ at an MOI of 3 (L); or PBS (−). The cells were harvested after 30 min of incubation at 37 °C. BALB/c mice were anesthetized by intraperitoneal injection with sodium pentobarbital (Somnopentyl, Schering-Plough Animal Health Corporation, Kenilworth, NJ, USA), and laparotomy was performed. Each mouse was injected with 1×10^6 adenovirus-infected BNL cells in a volume of 0.2 ml PBS containing 2% FBS or 0.2 ml PBS (−) via PV on day 0. The mice were sacrificed on day 21, and their liver tissues were weighed.

To determine whether CCL2/MCP-1 can enhance the antitumor effects of the HSV-tk/GCV system, BNL cells were infected with Ad-tk, Ad-MCP1 and Ad-LacZ at various MOIs: Ad-tk/Ad-MCP1 = 3/0.03 (T/M^{Low}), 3/0.3 (T/M^{Mod}) and 3/3 (T/M^{High}); Ad-tk/Ad-LacZ = 3/3 (T/L); and Ad-LacZ = 6 (N/L). BALB/c mice were anesthetized and each was injected via portal vein with 1×10^6 adenovirus-infected BNL cells on day 0, followed by intraperitoneal injection of 75 mg/kg/day ganciclovir on days 2–6. The mice were sacrificed on day 21, and the livers were removed and weighed. Additionally, in another series of experiments, the livers removed from the mice on days 1, 3, 7 and 14 were processed for immunohistochemistry and real-time quantitative reverse transcriptase-polymerase chain reaction (RT-PCR). Simultaneously, their splenocytes were tested for cytolytic activity against ^{51}Cr-labeled BNL cells.

Histopathological and immunohistochemical analysis

Liver sections were fixed in 10% zinc-buffered formalin and stained with hematoxylin and eosin (H&E). For histological evaluation, mouse livers were harvested, embedded in tissue-Tek® OCT embedding medium (Sakura Finetek, Torrance, CA, USA) and stored at −80 °C until use, except those stained for CD31 (Abcam, Cambridge, MA, USA), arginase I (Arg-I; BD Biosciences, Franklin Lakes, NJ, USA) and inducible nitric oxide synthase (iNOS; Thermo Fisher Scientific, Fremont, CA, USA). Cryostat sections of frozen tissues were fixed in cold acetone for 10 min and rinsed three times with PBS. The tissue samples used for CD31, iNOS and Arg-I staining were fixed in 10% phosphate-buffered formalin and embedded in paraffin. Following blocking of nonspecific tissue avidin and biotin with a blocking kit (Vector Laboratories, Burlingame, CA, USA), the slides were incubated with biotin-conjugated monoclonal antibody against Mac-1 (CD11b), CD4, CD8 (PharMingen, San Jose, CA, USA) or Arg-I or polyclonal antiserum against CD31 or iNOS for 30 min at room temperature. Biotin-conjugated rat IgG2b, kappa was used as the negative control. The reaction was visualized using a Vectastain® ABC Standard Kit (Vector Laboratories), followed by counterstaining with hematoxylin.

Real-time quantitative RT-PCR

The Frozen liver specimens containing necrotic liver tissues or tumor tissues were broken into fine pieces and total RNA was extracted from liver tissues using a ToTALLY RNA® kit (Ambion, Austin, TX, USA) in accordance with the manufacturer's instructions. Total RNA (1 μg) was reverse transcribed into cDNA using a SuperScript® first-strand synthesis system for RT-PCR (Invitrogen, Carlsbad, CA, USA). The first strand cDNA was used for real-time quantitative PCR using the ABI PRISM 7900 (Applied Biosystems, Foster City, CA, USA) with TaqMan® Master Mix (Applied Biosystems), and primers and probes for interleukin (IL)-4, IL-10, IL-12, IL-18, interferon (IFN)γ, vascular endolthelial growth factor (VEGF)-A and 18S ribosome (sequences available on request from the authors) (Applied Biosystems). The expression of cytokine mRNA in each sample was normalized relative to that of 18S ribosome mRNA.

Cytotoxic T lymphocyte assay (^{51}Cr release assay)

The cytolytic activity of mouse spleen cells was assessed by a ^{51}Cr release assay, as described previously [17]. Briefly, each treated mouse was sacrificed on day 14, splenocytes were harvested aseptically and mashed in alpha-minimal essential medium (MEM) medium (Gibco) with 10% FBS, and suspensions of single spleen cells were prepared. Spleen cells were cultured with mitomycin C (MMC; Sigma) (400 μg/4 ml, 1 mg/ml in HBSS) treated BNL or CT26 cells in complete alpha-MEM medium containing 10% FBS and 2.5% EL-4 culture supernatant (a source of T cell growth factor) for 5 days. Target cells consisted of 3×10^5 BNL cells labeled with 0.3 mCi $Na_2{}^{51}CrO_4$ (NEN Life Science Products, Boston, MA, USA) at 37 °C for 1 h. Effector spleen cells were incubated with 5×10^3 target cells in 96-well plates at various effector/target ratios for 4 h at 37 °C, and the ^{51}Cr released into the culture supernatants was quantified by scintillation

DOI: 10.1002/jgm

counting. Percent specific cytotoxicity was calculated according to the equation: [100 × (experimental release − spontaneous release)/(maximum release − spontaneous release)]. Spontaneous release was defined as the ^{51}Cr in the supernatant of target cells incubated for 4 h, and maximum release was defined as ^{51}Cr in the supernatant of target cells treated with 2% Triton-X. Experiments were performed three times and the results expressed as the mean ± SE. Tumor specificity was determined based on differences between BNL and CT 26 cells. All results presented are the means of triplicate assays.

Results

CCL2/MCP-1 production of recombinant adenoviruses *in vitro*

The production of CCL2/MCP-1 was evaluated by measuring the concentrations in culture media of BNL cells infected with varying MOIs of Ad-MCP1 and Ad-MCP1 plus Ad-tk by ELISA (Figure 1B). The production of CCL2/MCP-1 by cells infected with Ad-MCP1 increased in proportion to the MOI. Importantly, its production by Ad-MCP1 infected cells was not changed when these cells were further infected with Ad-tk (Ad-MCP1 plus Ad-tk), indicating that CCL2/MCP-1 production by Ad-MCP1 was not influenced by coinfection with Ad-tk in BNL cells. In addition, the functional properties of CCL2/MCP-1 produced by this rAd were defined previously [6–8].

Intrahepatic tumor development following transfer of HCC cells infected with recombinant adenoviruses

To evaluate the direct antitumor effect of CCL2/MCP-1 in an immunocompetent mouse model of IM, mice were injected via the PV with BNL cells infected with Ad-MCP1 or Ad-LacZ at various MOIs (Figure 1C). When whole livers were weighed on day 21, the weights of M^{Low} ($n = 4$), M^{Mod} ($n = 7$) and M^{High} ($n = 6$) were comparable to those of L ($n = 4$) mice, indicating that delivery of CCL2/MCP-1 gene did not promote or suppress the growth of tumor cells in this model.

To determine whether CCL2/MCP-1 gene delivery can potentiate the antitumor effects of the HSV-tk/GCV system, mice were injected with BNL cells infected with rAds (Ad-tk, Ad-MCP1 and Ad-LacZ) at various MOIs as described in the Materials and methods. Whole livers were weighed on day 21, and the weights of T/M^{Low} ($n = 14$), T/M^{Mod} ($n = 12$), T/M^{High} ($n = 11$) and T/L ($n = 10$) mice were compared with those of N/L ($n = 10$) mice. The reduction in liver weight for the T/L mice was a result of the HSV-tk/GCV system alone, and those for T/M^{Low}, T/M^{Mod} and T/M^{High} were a result of treatment in combination with CCL2/MCP-1. Mean ± SEM liver weight was significantly lower in T/M^{Low} mice than in T/L mice (3.91 ± 0.36 g versus 5.80 ± 0.58 g; $p < 0.01$) (Figures 1D and 1E) as a result of the reduced growth of implanted tumor cells in the former. By contrast, the increase in liver weight was not suppressed in T/M^{Mod} and T/M^{High} mice whose tumor cells had been treated with higher titers of Ad-MCP1. Thus, only low level CCL2/MCP-1 provided additional antitumor effects and these results indicate that delivery of adequate amounts of Ad-MCP1 enhanced the antitumor effects of the HSV-tk/GCV system against intrahepatic tumor cells.

Serial analysis of liver histology following tumor cell transfer

To monitor the course of tumor development following HCC cell transfer, mouse livers were harvested on days 1, 3, 7 and 14. Livers harvested on day 1 from all groups of mice injected with BNL cells showed multiple white patches on their surfaces. Histologically, hepatocyte degeneration and necrosis were observed in these lesions, suggesting that the reduction of PV flow by transferred tumor cells induced focal ischemic necrosis in the livers (Figure 2, closed arrowheads). Although the extent of necrosis was similar among all groups, inflammatory cell infiltration in the area of necrosis was greater in T/M^{Low}, T/M^{High} and T/L than in N/L mice. On day 3, cellular infiltration disappeared, and tumor cell growth was observed in areas surrounding the necrotic regions. On day 7, proliferation of viable tumor cells surrounding the necrosis was seen in the livers of N/L mice, with the necrotic tissues completely replaced by tumor cells. Tumor growth was moderately inhibited in T/L mice and greatly inhibited in T/M^{Low} mice. There was no difference between T/L and T/M^{High} mice (not shown). On day 14, the necrotic areas were almost absorbed in all mice. In N/L mice, the tumor cells grew progressively and the tumor masses became larger. Tumor volume was relatively lower in T/L than in N/L mice, although there was no significant difference between T/L and T/M^{High} mice. The greatest degree of tumor growth inhibition was observed in T/M^{Low} mice (Figure 2).

Recruitment of immune cells in liver

To evaluate the involvement of immune responses in the CCL2/MCP-1 associated enhancement of the antitumor effects of rAd expressing HSV-tk, we assessed the recruitment of Mac-1^+ monocytes/macrophages and $CD4^+$ and $CD8^+$ T lymphocytes immunohistochemically (Figure 3).

T/M^{Low} and T/M^{High} mouse liver tissues harvested on day 1 showed marked infiltration of Mac-1^+ cells in the necrotic areas induced by tumor cell injection (Figure 3A). Quantitative morphometric analysis showed that the numbers of Mac-1^+ cells were significantly higher in liver tissues of T/M^{Low} and T/M^{High} mice [mean ± SEM of 40 high power (×400) fields of necrotic liver

DOI: 10.1002/jgm

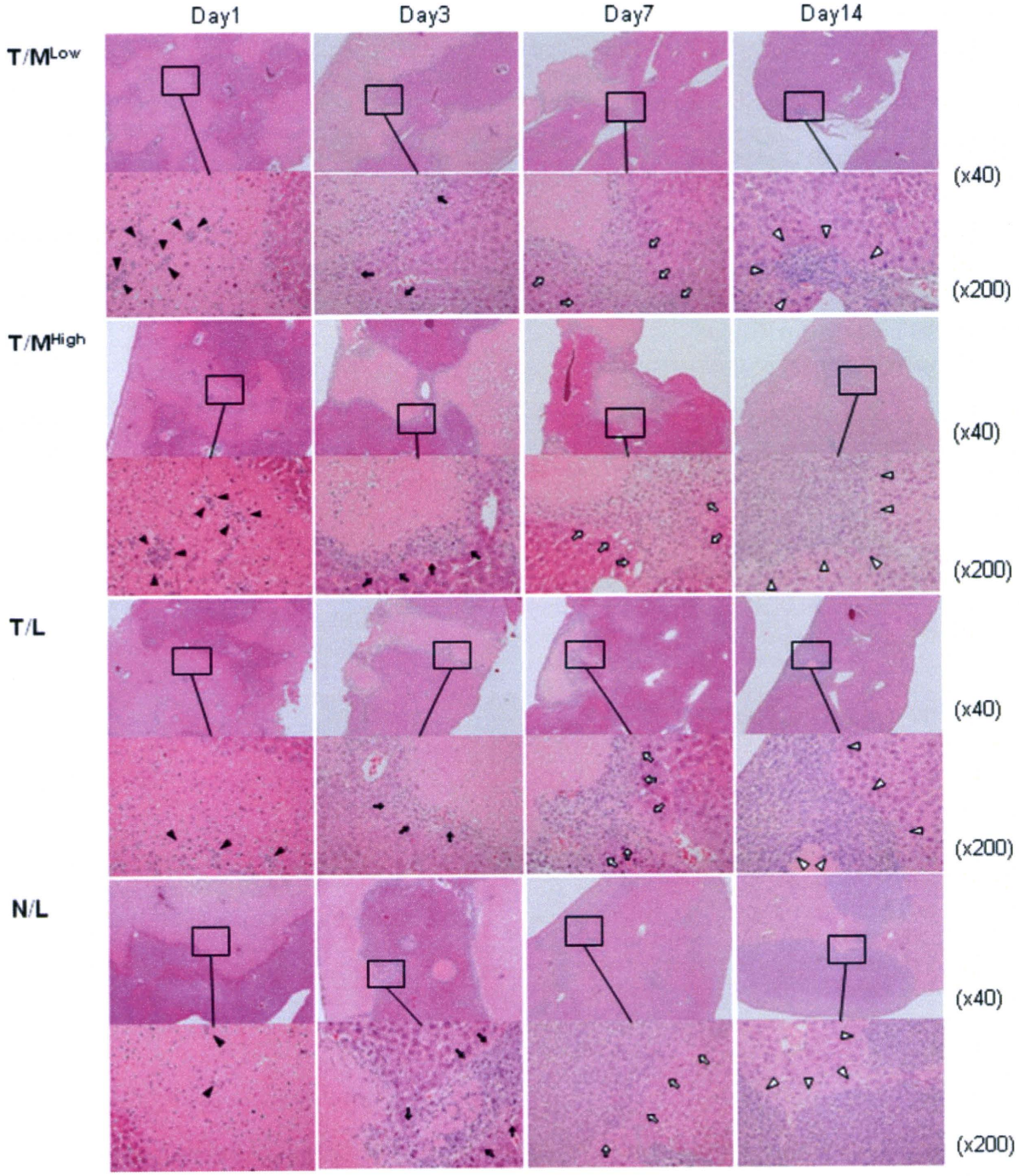

Figure 2. Serial analysis of liver histology following tumor cell transfer. Mouse liver tissues were harvested on days 1, 3, 7 and 14, and stained with H&E. On day 1, all mice injected with BNL cells showed multiple white patches on the liver surface (not shown). Histologically, hepatocyte degeneration and necrosis were observed in these lesions, suggesting that the reduction of PV flow by transferred tumor cells induced focal ischemic necrosis in the livers. The area of necrosis significantly infiltrated with inflammatory cells (closed arrowheads) was higher in T/M^{Low}, T/M^{High} and T/L mice than in N/L mice. On day 3, cellular infiltration disappeared and tumor cell growth (closed arrows) was detected in areas surrounding the necrotic regions. On day 7, tumor tissue enlarged and replaced the necrotic areas (open arrows). On day 14, the necrotic areas disappeared and tumor nodules eventually formed (open arrowheads). Original magnifications $\times 40$ and $\times 200$

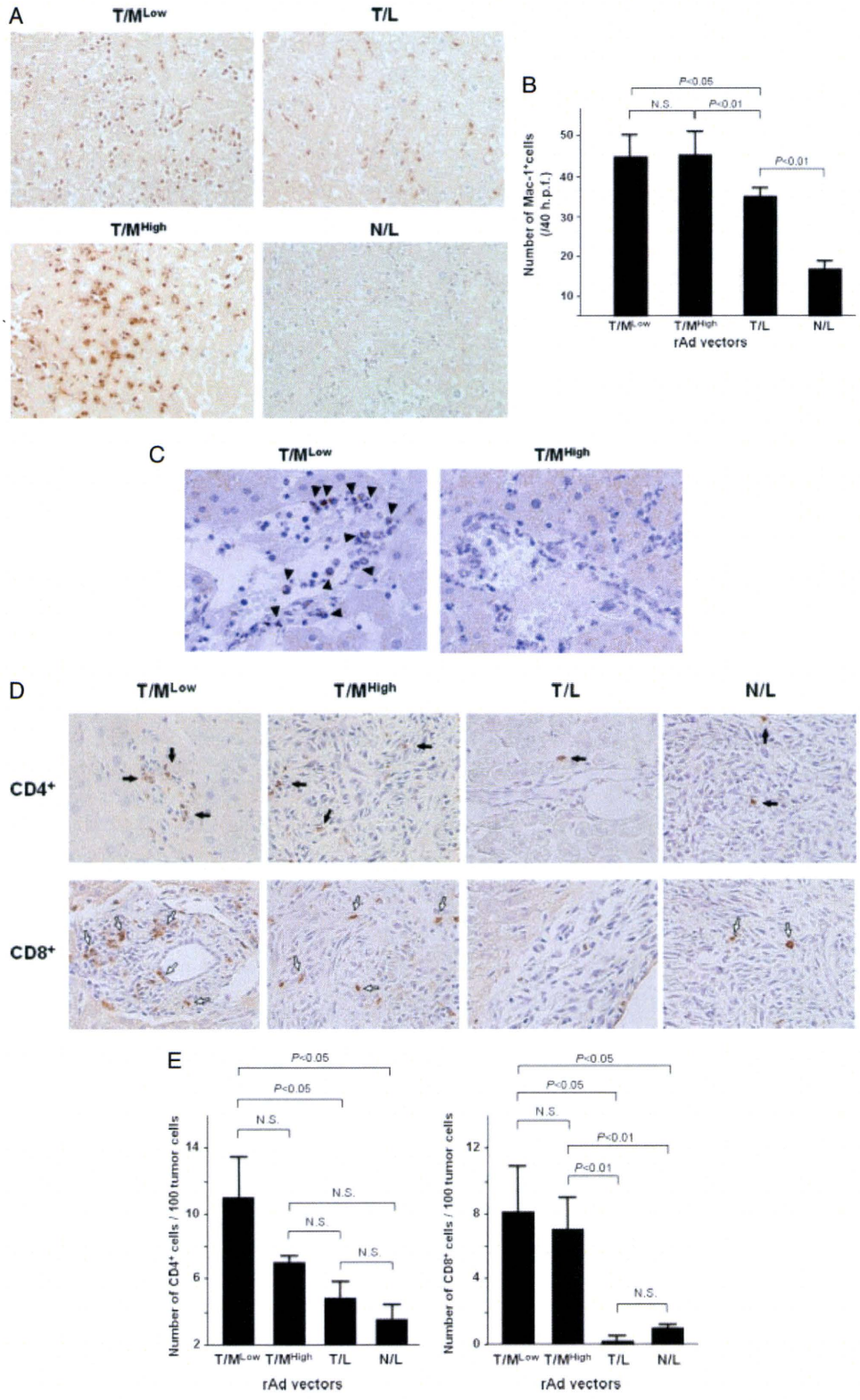

Figure 3. Immunohistochemical evaluation of monocyte/macrophage (A–C) and T cell (D, E) recruitment into liver tissues. (A) Monocyte/macrophage detection using anti-Mac-1 monoclonal antibody. Original magnification ×400. (B) Quantitative morphometric analysis of Mac-1$^+$ cells. (C) Immunohistochemical evaluation of the polarization towards M1 phenotype of recruited monocytes/macrophages using antibody against iNOS (closed arrowheads). (D) CD4$^+$ (closed arrows) and CD8$^+$ (open arrows) T cell detection. Original magnification ×400. (E) Quantitative morphometric analysis of CD4$^+$ and CD8$^+$ T cells

tissues: 46.5 ± 3.7 and 46.9 ± 3.7; $p < 0.05$ and $p < 0.01$, respectively] compared to T/L mice (35.2 ± 2.4). Macrophages can be activated not only by CCL2/MCP-1, but also by tumor cells treated with Ad-tk [6]. In T/L mice, these cells may induce moderate infiltration of Mac-1^+ cells (Figure 3B). These findings indicate that the codelivery of the HSV-tk and CCL2/MCP-1 genes was associated with a higher degree of infiltration of Mac-1^+ monocytes/macrophages during the initial period of tumor development. Additionally, to investigate whether the recruited monocytes/macrophages were polarized towards the M1 or M2 phenotype, we performed immunohistochemical analysis using antibodies against iNOS (M1) and Arg-I (M2) [17,18] (Figure 3C). The proportion of $iNOS^+$ (M1 subset) cells among the inflammatory cells was significantly higher in T/M^{Low} than in T/M^{High} mice [mean ± SEM number (per 100 inflammatory cells) of eight high power (×400) fields of necrotic liver tissues: 23.0 ± 2.7 and 10.8 ± 2.5; $p < 0.01$, respectively]. Arg-I^+ (M2 subset) cells were not specifically detected, most likely as a result of the large amounts of the enzyme present in liver tissues.

Similarly, liver tissues obtained on day 14 after HCC cell transfer were immunohistochemically analyzed for immune cell infiltration. In both T/M^{Low} and T/M^{High} mice, the tumor foci were heavily infiltrated by $CD4^+$ and $CD8^+$ T cells (Figure 3D). Quantitative morphometric analysis showed that the numbers of $CD4^+$ and $CD8^+$ T cells were higher in T/M^{Low} [mean ± SEM number (per 100 tumor cells) of eight high power (×400) fields of liver tissues: 11.1 ± 2.5 and 8.1 ± 2.7; $p < 0.05$ and $p < 0.05$, respectively] and T/M^{High} (7.1 ± 1.9 and 7.1 ± 0.7; not significant and $p < 0.01$, respectively) mice than in T/L mice (4.8 ± 1.1 and 0.3 ± 0.3, respectively) (Figure 3E). These results suggest that the antitumor activities in T/M^{Low} mice may be mediated not only by the activation of macrophages during the initial period of tumor development, but also by the induction of T cell-mediated immune responses during later periods.

Cytokine gene expression in liver

Mice injected with adenovirus-infected HCC cells were sacrificed on day 1 and their liver tissues were analyzed by quantitative real-time RT-PCR for the expression of mRNA encoding the cytokines IL-4, IL-10, IL-12, IL-18 and IFN-γ. IL-12 mRNA expression was induced to a greater extent in T/M^{Low} mice than in the other groups ($p < 0.05$). IL-18 mRNA expression tended to be high in the mice treated with CCL2/MCP-1, although these differences were not statistically significant (Figure 4). By contrast, IL-4, IL-10 and IFN-γ mRNA was not detected in any samples. These data suggest that infiltrating monocytes/macrophages induced by CCL2/MCP-1 may be activated to enhance the Th1-polarized responses that contribute to tumor immunity.

Microvessels in HCC

CCL2/MCP-1 has been shown to be associated with angiogenesis [19,20]. To understand the basis of the different antitumor effects observed in T/M^{Low} and T/M^{High} mice, we immunohistochemically stained microvessels within HCCs for CD31. We found that $CD31^+$ microvessels were markedly increased in 7-day tumor tissues of T/M^{High} mice relative to T/M^{Low} and T/L mice (Figure 5A). These results suggest that angiogenesis induced by large amounts of CCL2/MCP-1 may contribute to tumor growth in T/M^{High} mice.

VEGF gene expression in liver

Liver samples harvested on day 3 were analyzed for the expression of VEGF-A mRNA, which encodes an angiogenic factor that may promote tumor growth. Quantitative real-time RT-PCR showed that VEGF-A gene expression was induced to a greater extent in T/M^{High} mice (Figure 5B), suggesting that the CCL2/MCP-1 enhancement of antitumor effects may be offset by VEGF-induced angiogenesis.

Cytotoxic activities of splenocytes

To assess the cytotoxic activities of immune cells derived from mice injected with adenovirus-infected tumor cells, isolated and pulsed splenocytes were incubated with ^{51}Cr-labeled BNL cells in a standard 4-h cytotoxicity assay (Figure 6). Induction of cytotoxic T lymphocytes (CTLs) specific for BNL cells was higher in T/M^{Low} and T/M^{High} mice than in T/L (not significant) and N/L ($p < 0.01$) mice, and there was no significance difference between T/M^{Low} and T/M^{High} mice. Because the immunogenicity of viral vectors or transgene products is known to induce the unfavorable host immune responses, the detection of antitumor CTL activities may be influenced by the responses against rAd vector and HSV-tk [21–23]. Especially, CTL responses against HSV-tk appear to be induced in T/L, T/M^{Low} and T/M^{High} mice. Collectively, the data suggest that cytotoxic activity of CTLs may be enhanced by the codelivery of a suicide gene and CCL2/MCP-1, consistent with their *in vivo* enhancement of antitumor effects.

Discussion

In the present study, we have shown that combination gene therapy, using the HSV-tk/GCV system and CCL2/MCP-1 gene delivery, was effective for the treatment of HCC in a mouse model of IM. Delivery of an adequate amount of CCL2/MCP-1 enhanced the antitumor effects of the HSV-tk/GCV system against intrahepatic tumor cells. Necrotic areas induced by HCC tumor cell injection showed marked infiltration of $iNOS^+$

DOI: 10.1002/jgm